Low-PAPR OFDM-based Waveform for Fifth-Generation Cellular Communications

Yoav Levinbook, Doron Ezri, and Ezer Melzer

Huawei Technologies, Tel Aviv Research Center, 4 Ha'Harash St., Hod Hasharon, Israel
Email: (yoav.levinbook, doron.ezri, ezer.melzer)@huawei.com

***Abstract*—We introduce a novel technique for improving PA efficiency and coverage of communication links, especially advantageous for the uplink at high frequencies (cm/mm-Waves). The technique is based on a superposition of several DFT-s-OFDM (a.k.a. SC-FDM) signals, whose modulated symbol sequences and pulse shaping functions are coupled in a specially crafted manner. The resulting low-PAPR waveforms enable transmission with essentially no output power back-off (OBO), complying with rigid spectral requirements even when using PAs with highly non-linear behavior, expected from 5G cost-effective RF solutions. A relatively simple modification of a plain DFT-s-OFDM transmitter is required to support these waveforms. The inherent controlled ISI admits low-complexity BCJR-type demodulation, yet detection losses are small relative to the transmit power gains, thus yielding large net gains in link budget compared to competing transmission schemes.**

***Index Terms*—PAPR, power amplifier, DFT-s-OFDM, SC-FDM, 5G, PA efficiency, coverage enhancement.**

I. Introduction

The merit of using waveforms of low Peak-to-Average Power Ratio (PAPR) in wireless communication has long been recognized (see, *e.g.*, [1]). In a nutshell, due to the unavoidable non-linear behavior of the Power Amplifier (PA), which becomes more pronounced as the maximum transmission power is approached, an OBO must be taken in order to suppress Out-Of-Band Emissions (OOBE) and distortion of the transmitted signal. With any given PA, this OBO leads to loss of power efficiency and link range reduction. The required OBO typically increases with the PAPR of the signal.[1] This motivates the quest for low-PAPR waveforms, yet those enabling an efficient implementation of the communication system, namely supporting high throughput and/or capacity performance at a low cost of computational complexity.

In practice, the actual quantitative advantage gained from PAPR reduction depends on the properties of the PA (model) in use, particularly its non-linearity close to the saturation point. The technological challenge of producing linear, high-power and efficient PAs increases with the target deployment frequency. Thus, with recent years rising interest in utilizing cm- and mm-Wave spectra for next-generation communication [2]-[3], the PAPR issue becomes once again more relevant and acute.

The feasibility of *zero*-PAPR Single-Carrier (SC) signaling, namely the existence of constant-envelope (baseband) waveforms, is well known, often under the name Continuous Phase Modulation (CPM) [4]. However, it suffers from various disadvantages, mainly in the context of Multiple Access (MA) cellular communication systems.

Following the last decades' trends, 3GPP agreed to adopt OFDM-based waveforms for the emerging 5G New Radio (NR) standard [5] in all frequency ranges (up to 100 GHz). The OFDM[A] scheme has many advantages, but the high PAPR of the waveform is perhaps its most infamous shortcoming, which has led to enumerable proposals for different PAPR-reduction techniques [1],[6]. To enhance the uplink (UL) coverage of LTE, a particularly appealing such scheme was selected [7], called DFT-spread OFDM (DFT-s-OFDM), or SC-FDM[A] (especially when used in the MA context). The main usefulness of this scheme is that it maintains major advantages of OFDM[A], namely allowing FDMA and Frequency Domain Equalization (FDE) with (partly joint) multiuser processing at the receiver, while benefitting from the reduced PAPR of the UL waveform per user (which thus enjoys increased coverage and longer battery life). Yet, even for a low modulation order of the data QAM symbols, DFT-s-OFDM still exhibits quite a high PAPR, and further reduction is desirable.

An intriguing question arises, whether one can somehow "marry" the CPM and [DFT-s]OFDM schemes, creating an OFDM-based waveform with an extremely low PAPR. A scheme of that sort was proposed in the past in [8], where a CPM modulator output further undergoes DFT-s-OFDM modulation. We follow here a different path, a hint for which is found in Laurent's decomposition (and its generalizations thereof) of a CPM signal into a sum of SC "components". Inspired by these elegant results [9]-[10], we present in section II a new general scheme—dubbed *STORM*, which stands for *S*yn*T*hesis *O*f a nea*R*-constant *M*odulus waveform—where the CPM properties carry over (to some extent) to the SC realm, and further onto the DFT-s-OFDM framework (via the insertion of appropriate guard intervals). Implementation aspects of STORM, on both Tx and Rx sides, are discussed in section III, and section IV presents some performance results of the scheme in certain examples. Our conclusions are summarized in section V.

II. STORM Waveform Construction

The continuous time representation of the signal family we propose to consider is given in (1), where it is written in a form suitable for block-processing of M complex input modulated symbols $\{a_n\}_{n=0}^{M-1}$, one block at a time:

[1] The PAPR of a real (band-limited) RF signal is essentially 3 dB higher than the PAPR of the related complex baseband signal, which will be focused upon everywhere in the sequel.

978-1-5386-3169-0/17/$31.00 ©2017 IEEE

$$s_R(t)=\sum_{n=0}^{M-1}a_n\,\phi\big(t-nT\big)+\sum_{r=1}^{R}\sum_{n=0}^{M-1}b_{r,n}\,\varphi_r\big(t-nT\big),\qquad -T_g<t\le\widetilde{T}=MT. \tag{1}$$

This is a superposition of $R+1$ SC signals, constructible as DFT-s-OFDM waveforms with DFT size M (assumed even), within the duration $\widetilde{T}+T_g$ of a single OFDM symbol including a guard interval T_g of Cyclic Prefix (CP) type.[2] The first summand in (1) will be referred to as the *primary* component of the waveform, whereas the second is itself a sum of $R\ge 1$ *auxiliary* components, carrying the symbol sequences $\{b_{r,n}\}_{n=0}^{M-1}$, $r=1,2,\ldots,R$. Each component is shaped (at a common baud rate of $1/T$) by a pulse of its own, namely $\phi(t)$ and $\varphi_r(t)$ for the primary and r-th auxiliary component, respectively. Strictly speaking, these pulse shapes should be periodic with periodicity $\widetilde{T}$, and to ensure continuity of the signal at the boundaries between consecutive OFDM symbols some "smoothing" treatment (which we will not elaborate upon) should be performed.

The magic behind STORM is revealed only once another ingredient is added to the construction, in the form of a precise (theoretically, not necessarily in practice) dependence of the auxiliary symbol sequences and pulse shapes on the corresponding ones of the primary component. To introduce this "secret sauce", we are led to treat different modes of STORM separately, depending on the basic modulation order of the primary component.

A. Binary STORM (B-STORM)

Consider first the simplest (binary) mode, where the primary (info bearing) symbols a_n are taken from a π/2-rotated BPSK constellation, namely $a_n=e^{j\pi\alpha_n/2}$ where $\alpha_n\in\mathbf{Z}$ with $\alpha_n\equiv n\,(\mathrm{mod}\,2)$; particularly, without any loss of generality the α_n are assumed to obey the property $\delta_n:=\alpha_n-\alpha_{n-1}\in\{\pm 1\}$, where everywhere, here and in the sequel, index arithmetic should be understood as performed modulo M (*e.g.*, α_{n-1} stands for $\alpha_{(n-1)\,\mathrm{mod}\,M}$, *etc.*).

Introducing Λ, a natural number such that $R+1\le 2^{\Lambda}$, we construct the auxiliary symbol sequences according to

$$\forall r=1,2,\ldots,2^{\Lambda}-1,\quad b_{r,n}^{(\mathrm{B})}=a_n\prod_{\substack{m=1\\ d_{r,m}\neq 0}}^{\Lambda}\frac{a_{n-m-1}}{a_{n-m}},\qquad \text{where}\quad r=\sum_{m=1}^{\Lambda}2^{m-1}d_{r,m}\ ,\quad d_{r,m}\in\{0,1\}. \tag{2}$$

The dependence of the auxiliary pulse shapes (including their gains!) on the primary's is specified in (3), using relations that bear striking resemblance to those in (2):

$$\varphi_r^{(\mathrm{B})}(t)=\begin{cases}\phi(t)\displaystyle\prod_{\substack{m=1\\ d_{r,m}\neq 0}}^{\Lambda}\frac{\phi_{m+1}(t)}{\phi_m(t)} & \text{if}\quad \displaystyle\prod_{\substack{m=1\\ d_{r,m}\neq 0}}^{\Lambda}\phi_m(t)\neq 0\\ 0 & \text{otherwise}\end{cases} \tag{3}$$

where $\forall m,\quad \phi_m(t):=\phi\big(t+mT\big)$.

For (3) to be well-defined, $\phi(t)$ must satisfy certain conditions, otherwise the construction has to be carefully amended. To avoid obscuring the formalism unnecessarily, we will from now on restrict ourselves to real continuous nonnegative $\phi(t)$ having a compact connected support along the time axis, which is furthermore bounded within an interval of duration $(\Lambda+2)T$,[3] or more precisely that

$$\forall t\in(t_0,t_1),\ \phi(t)>0\,;\quad \lceil t_1/T\rceil-\lfloor t_0/T\rfloor\le\Lambda+2\,,\quad \text{where}\quad t_0=\min\operatorname{supp}\phi(t)\,,\ t_1=\max\operatorname{supp}\phi(t). \tag{4}$$

It follows from (3) and (4), that the auxiliary pulses are "shorter" than the primary one, satisfying

$$\operatorname{supp}\varphi_r^{(\mathrm{B})}(t)\subset(t_0,\,t_1-(\mu_r^{(\mathrm{B})}+1)T)\,,\quad \mu_r^{(\mathrm{B})}=\max_{\substack{1\le m\le\Lambda\\ d_{r,m}\neq 0}}m\,. \tag{5}$$

Our main theoretical result, presented here for the B-STORM case, is that the sum-representation (1) of the waveform is identically equal to the following product representation, when $R=2^{\Lambda}-1$:

$$s_{R=2^{\Lambda}-1}^{(\mathrm{B})}(t)=e^{\frac{1}{2}j\pi\alpha_{\nu(t)}}\,\phi_0(\tau)\prod_{m=0}^{\Lambda}\left(1+e^{-\frac{1}{2}j\pi\delta_{\nu(t)-m}}\,\frac{\phi_{m+1}(\tau)}{\phi_m(\tau)}\right), \tag{6}$$

where $\nu(t)=\lfloor t/T\rfloor,\ \tau=t-\nu(t)T,\ 0\le t<MT.$

The significance of (6) (where, without loss of generality, we used the convention $\lfloor t_0/T\rfloor=0$), is revealed once we consider the modulus of the waveform:

$$\left|s_{R=2^{\Lambda}-1}^{(\mathrm{B})}(t)\right|^2=\phi_0^2(\tau)\prod_{m=0}^{\Lambda}\prod_{\delta\in\{\pm 1\}}\left(1+e^{-\frac{1}{2}j\pi\delta}\,\frac{\phi_{m+1}(\tau)}{\phi_m(\tau)}\right), \tag{7}$$

where $\tau=t-\lfloor t/T\rfloor T\in[0,T),\ \forall t\in(0,MT).$

Namely, the modulus (envelope) of the waveform is a periodic function of time with periodicity T (within the OFDM symbol duration), which depends on the primary pulse shape $\phi(t)$ but is *completely independent of the data*! This, moreover, implies that the PAPR is deterministic and *a-priori* known given the primary pulse function (ignoring the short tailored segments of the signal at the boundaries between consecutive OFDM symbols, which have some rudimentary effect on the PAPR).

B. Quaternary STORM (Q-STORM)

In this mode the primary symbols a_n are taken from a π/4-rotated QPSK constellation; namely, $a_n=e^{j\pi\alpha_n/4}$ where

[2] This form can be generalized to other types of guard intervals, for instance a Unique Word (UW) where a fixed (pre-pulse-shaping) symbol sequence is inserted as a guard between symbol blocks, or alternatively degenerated into a pure multi-SC form by shrinking the guard duration to zero and taking *M* to be very large (covering a whole transmission burst).

[3] The guard interval is assumed to be longer, namely $T_g>(\Lambda+2)T$.

α_n are integers of alternating parity as in the binary case, but now their differences $\delta_n = \alpha_n - \alpha_{n-1} = 2\delta_n^{(0)} + \delta_n^{(1)}$ satisfy $\delta_n^{(i)} \in \{\pm 1\}$ $(i = 0,1)$ by convention. Here Λ is a nonnegative integer such that $R+1 \le 2 \cdot 3^{\Lambda}$, and the auxiliary symbol sequences are constructed according to

$$b_{1,n}^{(\mathrm{Q})} = \frac{a_n + a_{n-1}}{\left|a_n + a_{n-1}\right|}\left|a_n - a_{n-1}\right|; \quad \forall r = 2,3,\ldots,2\cdot 3^{\Lambda}-1:$$

$$b_{r,n}^{(\mathrm{Q})} = b_{r \bmod 2,n}^{(\mathrm{Q})} \prod_{\substack{m=1 \\ c_{\lfloor r/2 \rfloor,m}=1}}^{\Lambda} \frac{b_{1,n-m}^{(\mathrm{Q})}}{b_{0,n-m}^{(\mathrm{Q})}} \prod_{\substack{m=1 \\ c_{\lfloor r/2 \rfloor,m}=2}}^{\Lambda} \frac{b_{0,n-m-1}^{(\mathrm{Q})}}{b_{0,n-m}^{(\mathrm{Q})}}, \tag{8}$$

where $b_{0,n}^{(\mathrm{Q})} := a_n$, and $\forall \rho = 1,2,\ldots,3^{\Lambda}-1$,

$$\rho = \sum_{m=1}^{\Lambda} 3^{m-1} c_{\rho,m} \quad , \quad c_{\rho,m} \in \{0,1,2\}.$$

Reusing the notation introduced in (3) for the time-shifted primary (and first auxiliary) pulses, the auxiliary pulse shapes are constructed as follows:

$$\varphi_1^{(\mathrm{Q})}(t) = \widetilde{\phi}(t) := \sqrt{\phi_0(t)\phi_1(t)}$$

$$\forall r = 2,3,\ldots,2\cdot 3^{\Lambda}-1, \text{ denoting } \varphi_0^{(\mathrm{Q})}(t) := \phi(t), \tag{9}$$

$$\varphi_r^{(\mathrm{Q})}(t) = \begin{cases} \varphi_{r \bmod 2}^{(\mathrm{Q})}(t) \displaystyle\prod_{\substack{m=1 \\ c_{\lfloor r/2 \rfloor,m}=1}}^{\Lambda} \frac{\widetilde{\phi}_m(t)}{\phi_m(t)} \prod_{\substack{m=1 \\ c_{\lfloor r/2 \rfloor,m}=2}}^{\Lambda} \frac{\phi_{m+1}(t)}{\phi_m(t)} \\ \qquad \text{if} \quad \displaystyle\prod_{\substack{m=1 \\ c_{\lfloor r/2 \rfloor,m} \ne 0}}^{\Lambda} \phi_m(t) \ne 0 \\ 0 \qquad \text{otherwise} \end{cases}$$

Again, in (9) $\phi(t)$ is assumed to satisfy the same conditions described after (3), including (4). The pulse length characterization (analogous to (5)) now reads

$$\operatorname{supp} \varphi_r^{(\mathrm{Q})}(t) \subset (t_0,\, t_1 - (\mu_r^{(\mathrm{Q})}+1)T),$$
$$\text{where} \quad \mu_1^{(\mathrm{Q})} = 0, \quad \mu_{r>1}^{(\mathrm{Q})} = \max_{\substack{1 \le m \le \Lambda \\ c_{\lfloor r/2 \rfloor,m} \ne 0}} m \ , \tag{10}$$

and in analogy to (6), the sum-representation (1) of the "full-set" Q-STORM (when $R = R_{\Lambda} := 2\cdot 3^{\Lambda}-1$) is identically equal to the product representation (11), while the data-independence property of the modulus is expressed by (12):

$$s_{R_{\Lambda}}^{(\mathrm{Q})}(t) = e^{\frac{1}{4}j\pi\alpha_{\nu(t)}} \phi_0(\tau) \prod_{\substack{m=0, \\ i\in\{0,1\}}}^{\Lambda} \left(1 + e^{-\frac{1}{4}j\pi\delta_{\nu(t)-m}^{(i)}} \sqrt{\frac{\phi_{m+1}(\tau)}{\phi_m(\tau)}}\right), \tag{11}$$

$$\left|s_{R_{\Lambda}}^{(\mathrm{Q})}(t)\right|^2 = \phi_0^2(\tau) \prod_{m=0}^{\Lambda} \prod_{\delta\in\{\pm 1,\pm 3\}} \left(1 + e^{-\frac{1}{4}j\pi\delta} \sqrt{\frac{\phi_{m+1}(\tau)}{\phi_m(\tau)}}\right), \tag{12}$$

where $\nu(t) = \lfloor t/T \rfloor$, $\tau = t - \nu(t)T$, $\forall t \in (0, MT)$.

C. General remarks on the waveform design

We conclude this section by several remarks, which are applicable to both (binary and quaternary) modes introduced above (and possibly to other modes, not described here).

Beyond the elegance of the construction, which we believe is self-evident from the above formulas, any practical deployment of STORM clearly calls for an engineering trade-off between performance and complexity. The performance has (at least) two aspects, namely the PAPR (or OBO) gain, and the relative detection loss due to the ISI incorporated into the STORM waveform. Both are controlled, to a certain extent, by the choice of (i) primary pulse shape $\phi(t)$, (ii) the number R of auxiliary components included in the waveform on the Tx side, and (iii) their number R' $(\le R)$ attempted to be handled by the receiver. Their (adaptive and configurable) selection should take into consideration the deployment scenario, including the utilized PA (model) and enforced spectral requirements, such as the maximum transmission power, Spectral Emission Mask (SEM), Adjacent Channel Leakage Ratio (ACLR), Error Vector Magnitude (EVM), etc.

The implementation complexity is also strongly affected by the above three ingredients. Based on feasibility studies, a reasonable practical approach appears to be based on the existence of certain useful families of primary pulse shapes (with tunable parameters, depending on M, for instance), and restricting attention to $R' \le R = 1$. The case $R' = 0$, where the receiver altogether ignores the auxiliary component(s), is useful particularly in the B-STORM mode, where the power of the first dominant auxiliary component is already ~15 dB below that of the primary (and the targeted SNR of the BPSK-based scheme is relatively low, so that neglecting the weak auxiliary part of the signal is essentially unnoticeable).

In that respect, we further note that the structure of (3) and (9) is such that the relative gains $G_r = \int dt\, \varphi_r^2(t) / \int dt\, \phi^2(t)$ of the auxiliary components roughly decrease as the index r increases, so that (using the auxiliary indexing conventions implied by (2) and (8)) R serves as a natural "truncation parameter" of the B/Q-STORM waveforms (1). As implied by (7) and (12), limiting R to a smaller value than the size of the full set of auxiliary components (controlled by Λ, which in turn depends on the length of the primary pulse $\phi(t)$), destroys the property of data-independence of the waveform envelope. A certain PAPR penalty arises, as an unavoidable consequence of the abovementioned design trade-off.

III. STORM Implementation

Within the DFT-s-OFDM framework, a straightforward implementation of STORM can be performed in Frequency Domain (FD), as shown schematically in Fig. 1. The dark(er) blocks in the depicted diagram essentially implement a plain DFT-s-OFDM modulator; in other words, setting $R = 0$ (no auxiliary components), $Q = M$ and an all-1s Frequency Domain Spectral Shaping (FDSS) filter $g^{(0)}$, the output waveform degenerates into a SC-FDM baseband signal allocated over M contiguous subcarriers.

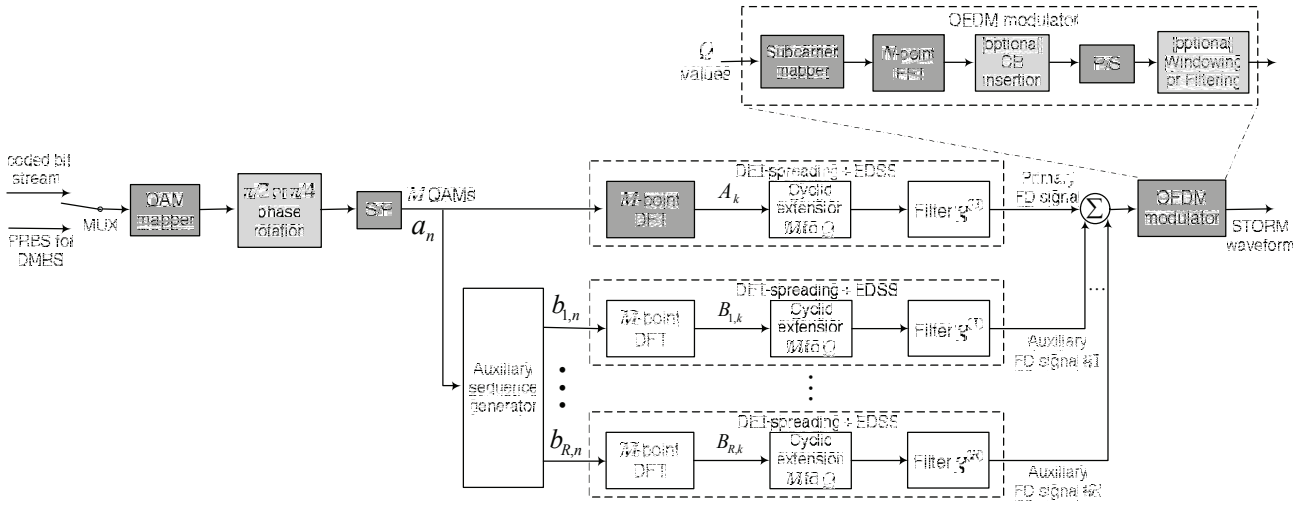

Fig. 1. Frequency domain implementation of STORM (baseband modulator block diagram)

The FDSS filters $g^{(r)},\ r=0,1,\ldots,R$ provide an approximate (discrete) FD representation for the primary (here $r=0$) and auxiliary pulse shaping functions, namely,

$$\begin{aligned}\phi(t) &\approx \sum_{k=0}^{Q-1} g_k^{(0)} e^{j\frac{2\pi}{MT}kt};\\ \varphi_r(t) &\approx \sum_{k=0}^{Q-1} g_k^{(r)} e^{j\frac{2\pi}{MT}kt},\quad \forall r=1,2,\ldots,R.\end{aligned} \tag{13}$$

The new design parameter Q introduced here, satisfying $M \le Q \le N$ (where N is the IFFT size of the OFDM modulator in Fig. 1), can be thought of as controlling the accuracy to which the filter taps $\{g_k^{(r)}\}_{k=0}^{Q-1}$ represent the corresponding Time Domain (TD) pulses. Clearly, for well-behaved primary pulse shapes, designed to support efficient transmission over M allocated subcarriers, most of the filter energy is concentrated over the M central taps with indices $k \in [\frac{Q-M}{2}, \frac{Q+M}{2})$, whereas the $Q-M$ taps at the edges decay sufficiently fast so as to comply with certain out-of-allocation spectral requirements (or, in some cases, occupy some excess bandwidth, which may or may not be utilized for transmission by another MA user).

To complete the description of Fig. 1, we note that the block "Auxiliary sequence generator" is responsible for implementing (2) and (8), in the B- and Q-STORM modes, respectively. Related to that, we also sketch a reduced-complexity (single-DFT) implementation of B-STORM when a single auxiliary component is included in the waveform: Exploiting the relative orthogonality of the primary and auxiliary symbol sequences, namely $\forall n,\ \mathrm{Re}(a_n^* b_{1,n}^{(\mathrm{B})}) = 0$, one can feed into a single DFT the "joint" sequence $\{a_n + jb_{1,n}^{(\mathrm{B})}\}_{n=0}^{M-1}$, and then split the DFT output to separately reconstruct the FD elements of the primary and auxiliary components (denoted by $\{A_k\}_{k=0}^{M-1}$ and $\{B_{1,k}^{(\mathrm{B})}\}_{k=0}^{M-1}$ in Fig. 1, respectively) before passing them each through its respective FDSS pipe. Finally, at the input to the whole block diagram we allude to the issue of DeModulation Reference Signal (DMRS) design, namely the insertion into the waveform of pilot symbols for channel estimation at the receiver. Doing so by MUX-ing together with the data bit-stream a Pseudo-Random Binary Sequence (PRBS), known to the receiver (both the sequence and its MUX-ing pattern), ensures homogeneity of the PAPR throughout the waveform; particularly, this approach prevents the DMRS from becoming the "PAPR bottleneck" of the overall waveform. However, other alternative DMRS designs are possible, but we will not elaborate here on them and on the whole issue, which involves many other (system-wise) considerations beyond the impacted link performance.

We turn next to discuss the receiver architecture, or more specifically the baseband demodulation algorithm. As already mentioned in the previous section, a clever primary pulse design leads in the case of B-STORM to auxiliary components which are very weak, and can be ignored by the receiver with a negligible detection loss. Furthermore, the primary pulse is effectively short, of duration $\sim 2T$, with a dominant ISI contribution caused by neighboring (consecutive) symbols which are relatively orthogonal: $\forall n,\ \mathrm{Re}(a_n^* a_{n-1}) = 0$. Consequently, the B-STORM demodulator can be implemented practically in a relatively simple manner, as shown schematically in Fig. 2.

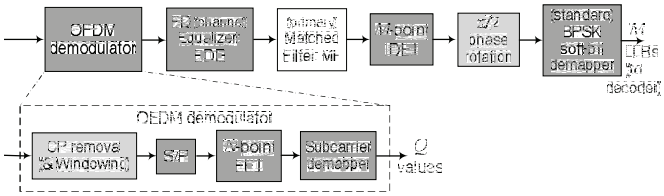

Fig. 2. Simplified (primary-only) B-STORM demodulator.

In the Q-STORM mode the situation gets more involved. Even the first (dominant) auxiliary component is relatively strong, only ~5 dB below the primary, and ignoring it at the receiver incurs an unbearable detection loss. A combined treatment of both primary and (first) auxiliary components is proposed in the block diagram drawn in Fig. 3.

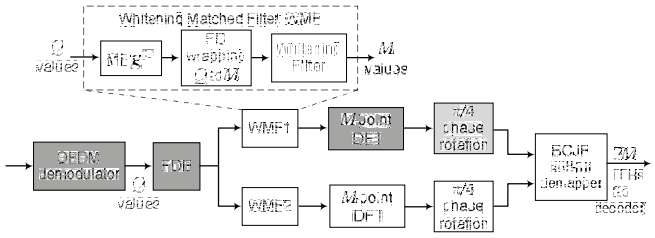

Fig. 3. Baseband block diagram of a Q-STORM demodulator.

The Whitening Matched Filter WMF1 in Fig. 3 attempts to extract the primary component. Its overall response, including an MF for the primary FDSS $g^{(0)}$, is designed to be causal and of minimal phase. In contrast, WMF2 is designed using an MF which is orthogonal to the primary's, followed by an appropriate whitening filter; as such, its overall response cannot be both causal and of minimal phase, in general. The output of both WMFs is fed, after performing IDFT and appropriate phase rotations, into a soft-bit demapper block whose role is to generate per-bit Log-Likelihood Ratios (LLRs). The demapper processes a *pair* of complex inputs at a time, carrying information extracted from both the primary and auxiliary signals, to yield two LLR outputs (per each transmitted QPSK symbol) at each step. The LLR sequence is then fed into a channel decoder (not shown in Fig. 3) for further decoding.

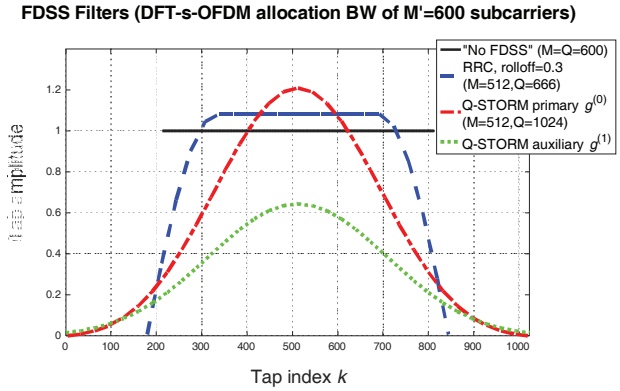

Fig. 4. FDSS filters: Q-STORM primary & auxiliary *vs.* RRC.

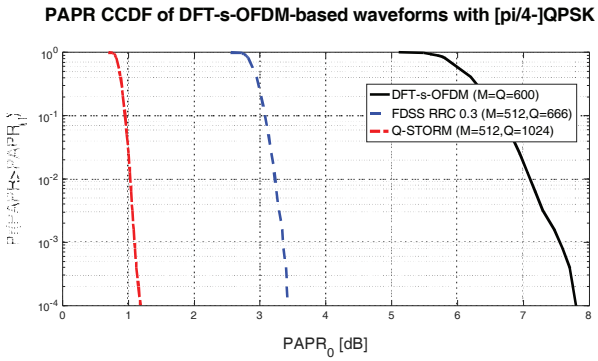

Fig. 5. PAPR of [π/4-]QPSK DFT-s-OFDM-based waveforms.

IV. Performance Evaluation

We focus here on the performance of a certain (single-auxiliary) variant of Q-STORM, adapted to LTE-like scenarios of wide bandwidth allocation.

Fig. 4 present the FDSS filter coefficients used for spectral shaping of the primary and auxiliary Q-STORM components, alongside the baseline plain DFT-s-OFDM rectangular FDSS (for reference), as well as a zero-ISI Root-Raised Cosine filter (RRC, here with roll-off 0.3) which is known to be useful for PAPR reduction purposes. All filter types in Fig. 4 assume allocation bandwidth of $M' = 600$ OFDM subcarriers, and the parameters M, Q of the RRC and Q-STORM filters (indicated in the legend) were selected in order to comply with the associated spectral containment requirements while at the same time optimize the overall link performance (see below).

The PAPR performance of these three QPSK-based schemes is shown in Fig. 5. The plotted PAPR CCDFs were generated by analyzing 10000 OFDM symbols whose CP length is ~7% of the symbol duration, consecutive OFDM symbols are tailored using Window OverLap and Add (WOLA) to suppress discontinuities at their boundaries, and $\times 4$ up-sampling is performed prior to the peak and average power measurements (as required for generating sufficiently reliable PAPR probability distributions). The large PAPR reduction offered by Q-STORM is evident from Fig. 5. As an aside, we remark that the π/4-rotation helps reducing the PAPR only in conjunction with spectral shaping, marginally affecting the PAPR of plain DFT-s-OFDM with QPSK.

To assess the practical benefits of Q-STORM, we turn to an evaluation of the attainable output power in the presence of a PA. We demonstrate the gains using the (memoryless) modified Rapp PA model specified in [11] while imposing the LTE User Equipment (UE) spectral requirements specified in [12].[4] Fig. 6 presents the Power Spectral Densities (PSDs) of the waveforms under consideration (here for $M' = 1200$ subcarriers, corresponding to full allocation in an LTE channel bandwidth of 20 MHz) after they pass through the PA model at the highest gain possible, still complying with the SEM, ACLR and EVM requirements. As indicated in the legend, Q-STORM can be transmitted with essentially zero OBO relative to the maximum Tx PA output power of 23 dBm, whereas the other schemes must take considerable backoffs.

Still, this is not end of story, since we must yet take into account the waveform detection performance at the receiver. Table I summarizes the evaluation results of the link performance of the three schemes under consideration. In all cases the same data rate is attempted to be delivered, namely 1 info-bit per time-frequency resource element (a single subcarrier within a single OFDM symbol). The detection loss of a waveform (w.r.t. the baseline DFT-s-OFDM) is the difference in Rx SNR required for maintaining a BLock ErrorRate (BLER) of 10%, for a Turbo encoded payload of

[4] For a meaningful incorporation of the SEM requirement, defined therein (cf. §6.6.2.1.1) in absolute terms [dBm/Hz] for a PC3 PA (max TRP of 23 dBm), the P_{sat} parameter of the PA model was up-scaled, which is equivalent to using several (identical) PAs by a single UE.

144,000 bits (spread over a subframe containing 12 OFDM symbols). AWGN channel is assumed, with ideal channel and noise estimation used by an MMSE-type FDE at the receiver. The Q-STORM detector employs the algorithm of Fig. 3, with a 16-state BCJR soft-bit demapper of reasonably low complexity (further complexity reductions are possible).

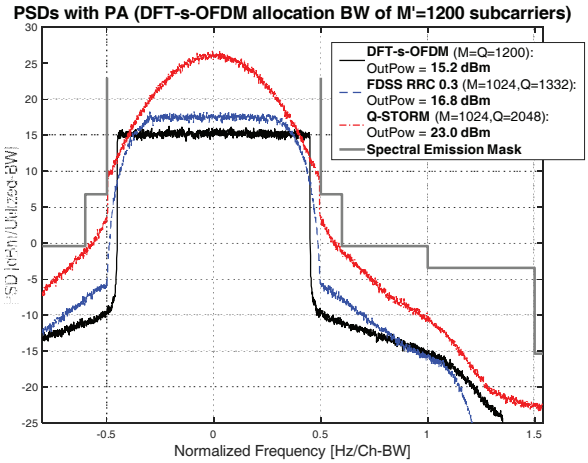

Fig. 6. PSDs and max output power of [π/4-]QPSK DFT-s-OFDM-based waveforms after passing through a PA model.

TABLE I
PERFORMANCE OF DFT-S-OFDM-BASED SCHEMES

Waveform: ($M'=1200$)	**DFT-s-OFDM** [baseline]	**FDSS RRC 0.3**	**Q-STORM**
DFT size (M)	1200	1024	1024
FDSS filter size (Q)	(1200)	1332	1332
Modulation	[π/4-]QPSK	π/4-QPSK	π/4-QPSK
Tx power [dBm]	15.2	16.8	23.0
OBO [dB] from 23dBm	**7.8**	**6.2**	**0.0**
ACLR [dBc]	30.0	30.0	30.0
EVM [%]	4.4	4.0	3.5
Limiting criterion	ACLR $\geq$ 30	ACLR $\geq$ 30	OBO $\geq$ 0
Code rate (Turbo)	0.5	0.586	0.586
Detection loss [dB]	**0**	**0.4**	**1.5**
Overall gain [dB]	**0**	**1.2**	**6.3**

The quoted detection loss of the DFT-s-OFDM with FDSS scheme is essentially due to the required increase (by a factor of $M'/M = 1200/1024$) in the code rate. The extra loss suffered by Q-STORM is due to its inherent ISI. Despite the non-negligible detection loss, by virtue of its large output power gain, Q-STORM exhibits an overall gain of ~6 dB in the considered scenario, which translates into a significant coverage enhancement. This gain is maintained also when practical channel estimation is invoked, based on DMRS which preferably undergo the same shaping like the data (in order not to require higher OBO), as long as the channel is not too selective in frequency (as expected in LOS-dominant mm-Wave deployments) and the code rate is not too high.

V. CONCLUSION

We introduced a novel construction (*STORM*) of waveforms which are generated as a superposition of specially-crafted dependent SC[-FDM]-based signals. At least when the modulation order of the underlying data symbols is low (*e.g.*, BPSK or QPSK), we demonstrated the feasibility of using the general construction to produce waveforms of very low PAPR, in particular with weak (or even completely no) dependence on the input data for transmission. This property is achieved via a low-complexity predefined implementation, in contrast to many other known PAPR-reduction techniques which require on-the-fly (data-dependent, often iterative) costly computations at the transmitter. The reduced PAPR translates into larger output PA power (and increased PA efficiency), and thus offers high potential for coverage enhancement, especially when the utilized PA exhibits high levels of non-linearity, as expected in practical 5G deployments at mm-Wave frequencies (certainly in the uplink case).

The actual overall gains of the scheme must take into account the detection performance of the waveforms, which depends on the controlled ISI (an integral part of STORM) as well as on the receiver architecture. The presented results show that STORM can yield high overall gains, doubling the link range in certain scenarios, even when deploying suboptimal receivers of reasonable complexity.

REFERENCES

[1] G. Wunder *et al.*, "The PAPR problem in OFDM transmission: New directions for a long-lasting problem," *IEEE Signal Processing Magazine*, vol. 30, no. 6, pp. 130-144, November 2013, and references therein.

[2] Y. Niu *et al.*, "Survey of millimeter wave communications (mmWave) for 5G: Opportunities and challenges," *Wireless Networks*, vol. 21, no. 8, pp. 2657-2676, April 2015.

[3] 3GPP TR 38.913, V14.2.0, "Study on Scenarios and Requirements for Next Generation Access Technologies," March 2017 (§10.1.6).

[4] C. E. Sundberg, "Continuous phase modulation," *IEEE Commun. Magazine*, vol. 24, no. 4, pp. 25-38, April 1986.

[5] 3GPP TS 38.211, V0.1.0, "NR; Physical channels and modulation," June 2017.

[6] Y. Rahmatallah, and S. Mohan, "Peak-to-average power ratio reduction in OFDM systems: A survey and taxonomy," *IEEE Communications Surveys & Tutorials*, vol. 15, no. 4, pp. 1567-1592, March 2013, and references therein.

[7] 3GPP TS 36.201, V8.3.0: "E-UTRA; LTE Physical Layer – General Description," March 2009.

[8] M. P. Wylie-Green, E. Perrins, and T. Svensson, "Introduction to CPM-SC-FDMA: A novel multiple-access power-efficient transmission scheme," *IEEE Trans. Commun.*, vol. 59, no. 7, pp. 1904-1915, July 2011.

[9] P. A. Laurent, "Exact and approximate construction of digital phase modulations by superposition of amplitude modulated pulses," *IEEE Trans. Commun.*, vol. 34, no. 2, pp. 150-160, February 1986.

[10] U. Mengali, and M. Morelli, "Decomposition of M-ary CPM signals into PAM waveforms," *IEEE Transactions Inform. Theory*, vol. 41, no. 5, pp. 1265-1275, September 1995.

[11] IEEE P802.11 Wireless LANs, doc. 802.11-15/0866r4, "TGay Evaluation Methodology," January 2016 (§2.2.3).

[12] 3GPP TS 36.101, V8.27.0, "E-UTRA; User Equipment (UE) radio transmission and reception," March 2016.